

Many-body luminescence from highly excited quantum-confined structures

T. V. Shahbazyan

Department of Physics, Jackson State University, Jackson, MS 39217

M. E. Raikh

Department of Physics, University of Utah, Salt Lake City, UT 84112

Abstract

We review recent results on many-body effects in the luminescence from semiconductor nanostructures. Many-body luminescence from highly excited quantum-confined structures is *conceptually* important topic since a new parameter, a level spacing, plays a crucial role. This spacing is *not* merely a discretization of the bulk luminescence spectrum, as it could seem. The *interplay* of finite spacing with interactions (even weak) results in a highly nontrivial sequence of emission lines, their heights revealing the many-body correlations in the system. Here the complex structure of the emission spectrum, resulting from the shakeup processes in many-particle (but finite) system, is demonstrated for a confined electron-hole system of a particular geometry, in which the interacting carriers are confined to a ring. For this geometry, the Luttinger liquid theory allows one to exactly calculate the *intensities* of all many-body spectral lines. The *positions* of the lines are governed by the relation of the level spacings for electrons and holes. While close to the emission threshold the interactions cause only weak shakeup satellites of the single-particle lines, away from the threshold the discrete luminescence spectrum is completely dominated by the many-body transitions. We describe the Luttinger liquid approach for calculations of optical spectra in finite one-dimensional systems. The calculations are preceded by a detailed review of experimental and theoretical work on many-body luminescence from various infinite systems. We also review the current status of the experimental and theoretical research on quantum nanorings.

I. INTRODUCTION

Luminescence from zero-dimensional objects (quantum dots) is one of the highlights in physics of nanostructures which emerged during the last decade. Early papers (see, e.g., Refs. [1, 2], and the review article Ref. [3]) reported the PL spectra consisting of "zero-width" luminescence lines. High surface density of quantum dots caused an ambiguity in assigning of these lines. In the later studies the emission from a *single* dot was resolved. This progress[4] has permitted the luminescence spectroscopy of individual dots with controllable exciton population determined by the excitation intensity.

Since many-body optical transitions in zero-dimensional objects were demonstrated experimentally, it is important to assess this phenomenon from the perspective of the well established field of many-body luminescence. This is accomplished in the present chapter. Below we review the many-body luminescence in various systems studied to date experimentally and theoretically. We then demonstrate that many-body luminescence from highly excited zero-dimensional objects has unique features due to *large* number of *discrete* lines. This discreteness *unravels* the many-body correlations that are otherwise masked in the continuous spectrum of luminescence from infinite systems. We describe in detail the emergence of such correlations for a particular nanostructure geometry – semiconductor nanorings – using the Luttinger liquid approach for quasi-one-dimensional finite-size systems.

II. SPECTROSCOPY OF MANY-BODY PROCESSES

A. Shakeup effects in optical spectra of many-electron systems

Shakeup represents a fundamental many-body effect that takes place in optical transitions in many-electron systems. In such systems, an absorption or emission of light is accompanied by electronic excitations in the final state of the transition. The most notable shakeup effect is the Anderson orthogonality catastrophe[5] in the electron gas when the initial and final states of the transition have very small overlap due to the readjustment of the Fermi sea electrons in order to screen the Coulomb potential of photoexcited core hole. Shakeup is especially efficient when the optical hole is immobilized, and therefore it was widely studied in conjunction with the Fermi edge singularity (FES) in metals [6, 7, 8] and doped semiconductor quantum wells [9, 10, 11, 12, 13, 14, 15]. Comprehensive reviews of FES and related issues can be found in Refs. [16, 17].

1. Shakeup processes in electron gas

The long-time dynamical Fermi sea response to a sudden appearance of the optical hole Coulomb potential can be viewed as a dressing of that hole by the low-energy Fermi sea excitations. This leads to the power-law infrared divergence in the hole density of states[16, 17]. In three-dimensional (3D) electron gas, the only low-energy excitations are the Fermi sea electron-hole pairs, and, therefore, close to the absorption onset, the electron-electron interactions are usually neglected. Incorporation of electron-electron interactions gives rise to the plasmon satellites [8, 18], which are somewhat similar to the low-energy phonon replicas. Each of these satellites also represents a power-law divergence at the energy $n\omega_p$, where ω_p is the bulk plasmon frequency (we set $\hbar = 1$) and n is an integer. In contrast, in

low-dimensional electron systems, the plasmon is gapless, so the shakeup of single-particle and collective excitations must be treated on equal footing. In 2D electron gas, where the plasmon dispersion is $\omega_q \propto \sqrt{q}$ for small q , the plasmon shakeup leads to a narrowing of the main singularity and to an additional structure at energies corresponding to the plasmon bandwidth [19]. Note, however, that plasmon effect is negligible near the Fermi edge because of a much smaller 2D plasmon density of states at low energies as compared to that of electron-hole pairs. In contrast, the role of plasmon shakeup is much more important in 1D electron systems, where the plasmon dispersion is linear. Since the electron dispersion in the vicinity of the Fermi level is also linear, single-particle and collective excitations are intertwined, forming a strongly correlated electron liquid. The exact solution of the 1D FES in the long time limit, which was carried out using the Luttinger model[20], revealed that the power-law exponent is determined by both electron-hole and electron-electron interactions [21, 22, 23].

2. Magnetoplasmon shakeup in semiconductor quantum wells

Shakeup processes are quite pronounced in luminescence from a 2D electron gas in a perpendicular magnetic field. In such systems, the single-particle energy spectrum represents a staircase of equidistant Landau levels (LLs) separated by the cyclotron energy ω_c . Here, a recombination of an interband electron-hole pair is accompanied by electronic transitions across the cyclotron gap. Shakeup satellites, corresponding to excitation of magnetoplasmons as well as to inter-LL Auger transitions, were observed in a number of experiments [24, 25, 26, 27, 28, 29, 30, 31, 32], in agreement with earlier theoretical predictions [33, 34, 35]. The general expression for the ground state luminescence intensity has the form[16]

$$I(\omega) \propto \sum_f C_f \delta(\omega + E_f - E_i), \quad (1)$$

where E_i and E_f are initial (ground) and final state energies and the oscillator strengths C_f are given by the square of the dipole matrix element. In the absence of interactions, the recombination act does not perturb the system and so the initial and final state energy difference is simply $E_g + (\omega_c^e + \omega_c^h)/2$, where both electron and hole belong to the lowest LL[36]. In the presence of interaction, the inter-LL magnetoplasmon satellites appear in the lower tail of the spectrum at frequencies that are multiples of the electron cyclotron energy, ω_c^e . Note that in doped quantum wells, the actual separation between LLs is less than ω_c^e due to the exchange effects, so the magnetoplasmon energy lies above that of single-particle transitions. Magnetic-field dependence of the oscillator strengths C_f is determined by several factors. For even integer filling factors, $\nu = 2\pi l^2 n_e$ (n_e is electron concentration and l is the magnetic length), the screening of Coulomb interaction by the electron gas is strongly suppressed, resulting in the enhancement of satellite amplitudes[30, 33]. Another widely-observed feature was a suppression of satellite peaks for filling factor $\nu < 2$, i.e., when only the lowest LL is occupied. Such a suppression originates from the electron-hole symmetry in the lowest LL[37], which results in a cancellation of the electron and hole final state Coulomb matrix element contributions to C_f [36]. In the valence band, similar inter-LL shakeup processes were observed in p -doped [38, 39] GaAs quantum wells.

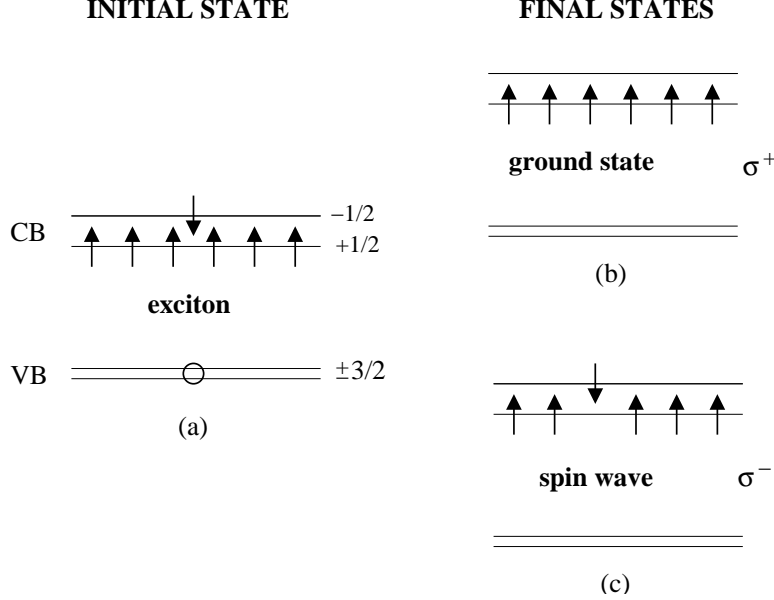


FIG. 1: Luminescence from $n = 0$ LL at filling factor $\nu = 1$. Recombination of initial interband exciton (a) can result either in ground state for σ^+ polarization (b), or spin wave shake up for σ^- polarization (c).

3. Spin wave shakeup in quantum Hall ferromagnets

In one-side modulation-doped quantum wells, the aforementioned electron-hole symmetry is violated due to the spatial separation between the electron and valence hole planes that is caused by the interface potential. In such samples, polarization-dependent spectral redshifts were reported as the filling factor was swept through integer values [28, 29, 31, 40, 41, 42, 43]. These redshifts were attributed to the competition between interband Coulomb binding and electron self-energies in the final state [44, 45]. For example, for $\nu = 1^-$, the initial state represents a valence hole and a full spin-polarized LL in conduction band which is negatively charged in order to compensate the positive hole charge. A recombination leaves a hole in the conduction band LL with exchange energy $E_{ex} = \sqrt{\pi/2} e^2 / \kappa l$ (κ is the dielectric constant). For $\nu = 1^+$, the initial state consists of an interband magnetoexciton made up from a valence hole and an electron in the upper (spin-up) polarized LL, with a binding energy E_0 . Then the removal of an electron from the lower (spin-down) polarized LL leaves a *spin wave* in the final state of the transition with just the Zeeman energy (see Fig. 1). The difference between below and above $\nu = 1$ final state energies is thus $E_{ex} - E_0 > 0$ in such asymmetric structures, which accounts for the redshift. A similar analysis was applied to the redshifts observed near $\nu = 2$ filling factor [28, 29, 31, 40, 43]. In single heterojunctions, systematic studies of the electron-hole separation as a function of carrier concentration were carried out in Ref. [46].

The shakeup of spin waves, mentioned above, has been observed prominently in the magnetoluminescence spectra at filling factors close to 1, 3, and 5 [31, 40, 41, 42, 43, 47]. At $\nu = 1$, an asymmetric broadening of the luminescence peak with additional spectral weight on low energy side was observed for σ_- -polarized light [47]. The origin of this broadening was explained as follows [44]. For σ_+ polarization, the recombination of an exciton, made

up from a valence hole and an $n = 1$ LL electron, leaves the 2DEG in the ground state, resulting in narrow emission peak (see Fig. 1). For σ_- polarization, the final state is a spin-wave with momentum q equal to that of the exciton before the recombination, so the lineshape at low energies is determined by the difference between the dispersions of a spin wave and an exciton. Furthermore, for filling factors $\nu = 3$ and 5, a splitting of the ground state luminescence peak was observed for σ_- polarization[31, 40]. This splitting, greatly enhanced at low temperatures, was attributed to the Anderson-Fano resonance in the final state that originated from the destructive interference between the hole, left in the conduction band LL after recombination, and the continuous spectrum of the spin wave [45].

B. Shakeup of electron excitations in few-particle systems

1. Shakeup satellites in atoms

In atoms and molecules, shakeup satellites, corresponding to internal electronic transitions, are routinely observed using photoelectron and resonant Raman spectroscopy. In particular, shakeup satellites can be observed in the two particle spectrum, i.e., when two holes are left in the final state of an atom after electron emission. Satellite's strength can be strongly enhanced in the presence of a resonant intermediate state. For example, in copper atoms, the incident photon can first excite the core 3p electron to the 4s shell; the core hole then decays to the 3d shell through the Auger process (with electron ejected from 3d shell) leaving two 3d holes in the final state[48]. For recent reviews of extensive literature the reader is referred to Refs. [49, 50]).

2. Many-body luminescence lines in single quantum dots

In semiconductors, multiple emission lines have been recently observed in the luminescence from single self-assembled quantum dots [51, 52, 53, 54, 55, 56, 57, 58, 59, 60, 61, 62, 63, 64]. At low excitation intensities, the luminescence from a dot is dominated by the ground state single-exciton recombination (i.e., from lowest size-quantization levels in conduction and valence bands). Upon increasing the excitation intensity, as the number of excited carriers increases, new emission lines appear in the luminescence spectrum. These lines were interpreted in terms of recombination within many-exciton complexes. One reason for the emergence of additional lines is that the carriers, constituting a complex, occupy higher size-quantization levels. Another reason, is that the interactions between strongly confined photoexcited carriers lift the *degeneracies* within the final many-body states. The latter mechanism was addressed in Refs. [55, 56, 63, 64, 65] for the situations with[63, 64, 65] and without[55, 56] orbital degeneracy of single-particle states. The calculations carried out in Refs. [55, 56, 64, 65] predicted the splittings of luminescence lines, originating from different many-body final states, to be of the order of matrix element of the interaction potential. The actual positions of these lines, corresponding to interband transitions between states with the *same* size-quantization quantum numbers, reproduce quite accurately the experimental PL spectra of Refs. [55, 56, 57, 60] (for up to $N = 16$) and of Ref.[59, 64] (for $1 \leq N \leq 6$). The third type of additional lines were identified with the transition energies corresponding to *different* size-quantization levels[55, 56]. Such transition energies point to shakeup processes in a *confined electron-hole system*, when the recombination of an

electron-hole pair is accompanied by internal excitations within the exciton multiplex.

3. Density dependence of optical spectra

The evolution of optical spectra with increasing electron gas density was studied both in metals [66] and in semiconductor quantum wells [67, 68, 69, 70]. In the absence of conduction electrons, the absorption spectrum is characterized by two peaks – a sharp exciton line well separated from a step-like onset of continuum states. In metals, the presence of conduction band electrons asymmetrically broadens the exciton peak according to $(\omega - \omega_1)^{-\alpha}$ with α decreasing in the (0,1) interval as the electron concentration increases, while the step-like continuum edge also acquires a power-law shape, $(\omega - \omega_2)^\beta$ with β increasing with concentration in the (0,3) interval [66]. In contrast, in semiconductor quantum wells with low electron concentration, the ground state represents a negatively charged exciton, X^- , formed as a result of the binding of an additional conduction electron by a photoexcited interband electron-hole pair [71, 72, 73]. This leads to an emergence of the exciton peak (X), corresponding to ionized X^- , located between the ground state X^- peak and the absorption onset at the Fermi energy E_F [67]. The evolution of absorption/emission spectra with increasing 2D electron gas concentration was traced in Refs. [68, 69, 70]. As the electron concentration increases, so does the separation between X^- and X peaks; at the same time, the oscillator strength of X is reduced as the exciton binding energy becomes smaller than E_F . The lineshape undergoes a qualitative change from exciton-like to continuum-like as concentration exceeds some characteristic value [68, 69, 70]. In particular, above that value, the absorption spectrum develops higher-energy tail corresponding to the shakeup transitions. It was also noted [70] that, in a weak magnetic field, the character of shakeup satellites in the low-energy tail of luminescence spectrum changes: for higher electron concentrations, the magnetic field dependence of satellite peak separation indicates excitation of magnetoplasmons, as opposed to single-particle transitions for lower concentrations [74, 75].

C. Shakeup effects in highly excited nanostructures

All the above studies of the optical spectra evolution from few- to many-particle cases were carried out for *infinite* systems, i.e., those with *continuous* excitation spectrum (at zero field). In such systems, the shakeup processes play increasingly important role, as indicated by the emergence of the power-law behavior at higher electron concentrations. However, these studies provide no insight into the structure of many body states at the onset of transition from discrete to continuous spectrum. In *finite-size* systems with *discrete* excitation spectrum, the oscillator strengths of satellite peaks characterize the amplitudes of corresponding shakeup transitions which, in turn, are determined by the interaction matrix elements as well as by statistical weights of the contributing many-body processes. With increasing system size (at constant carrier concentration) new shakeup satellites should emerge due to an increase in the number of many-body states available for non-radiative transitions. In fact, the positions and magnitudes of shakeup satellites represent the *fingerprint* of the system many-body excitation spectrum. With further increase in the system size, the satellite peaks should eventually merge; the energy dependence of their peaks *envelope* should then follow the power-law lineshape of the continuous spectrum for the corresponding infinite system.

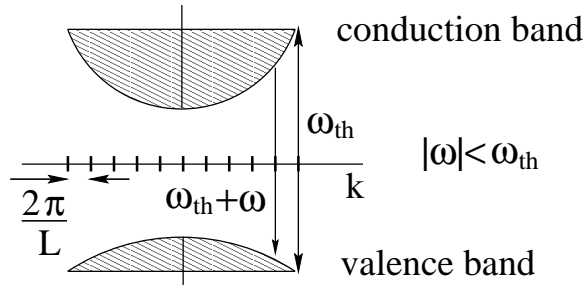


FIG. 2: In highly-excited quantum-confined structures, photoexcited carriers form electron and hole Fermi seas in conduction and valence bands, respectively; ω_{th} is the energy distance between the corresponding Fermi levels. Recombination of electron-hole pairs, belonging to space-quantization energy levels, gives rise to discrete lines in the luminescence spectrum.

In the following, we consider in some detail the transition from discrete to continuum spectra for the case of luminescence from highly excited semiconductor nanostructures. We will restrict ourselves to undoped semiconductors so that all carriers in conduction and valence band are optically excited. The luminescence is preceded by a fast carrier relaxation[76], so the recombination takes place when the electron and hole gases are in their respective ground states. In quantum wells, luminescence from high-density optically created electron-hole gases was studied in Refs. [77, 78, 79]. In confined structures, such as quantum dots, electrons and holes fill size-quantization energy states up to their respective Fermi levels in conduction and valence bands (see Fig. 2). We will only consider the higher-frequency domain of the emission spectrum corresponding to frequencies not too far from the electron and hole Fermi edge's separation. For a noninteracting system, the emission lines would correspond to the transitions between size-quantization levels in conduction and valence bands which obey the selection rules, so the the general expression (1) becomes

$$I(\omega) \propto \sum_n C_n \delta[\omega + (\Delta_1 + \Delta_2)n], \quad (2)$$

where Δ_1 and Δ_2 are level spacings for electrons and holes; C_n are the oscillator strength which depend on n only *weakly* ($\omega < 0$ is measured from the Fermi edge).

As discussed above, the many-body transitions due to the interactions between carriers change qualitatively the form of the spectrum. Namely, a removal of an electron-hole pair shakes up the respective Fermi seas by causing them to emit Fermi sea excitations. Since in a *finite-size* system, the energies of excitations are *quantized*, such a shakeup would lead to the following spectrum,

$$I(\omega) \propto \sum_{mn} C_{mn} \delta(\omega + m\tilde{\Delta}_1 + n\tilde{\Delta}_2), \quad (3)$$

rather than Eq. (2). Here $\tilde{\Delta}_1$ and $\tilde{\Delta}_2$ are the level spacings renormalized by interactions. The emission lines with $m \neq n$ are, thus, shakeup satellites. All the information about many-body correlations in the system is encoded in the oscillator strengths C_{mn} . In fact, C_{mn} , being governed by interactions, are *strong* functions of m and n .

In general, the evaluation of coefficients C_{mn} presents a major challenge. Remarkably, in the case of 1D systems, C_{mn} can be calculated *analytically* when the number of carriers, N , is large, but the emission spectrum is still discrete[80]. Such systems have recently

been manufactured and will be reviewed in the next section. In this case, the luminescence from 1D electron-hole system can be described within the finite-size Luttinger liquid formalism[20]. Note that the Luttinger liquid model was employed earlier for calculations of the Fermi-edge optical properties of *infinite* 1D systems (with and without defects) in Refs. [21, 22, 23, 81, 82].

D. Semiconductor nanorings

Properties of electron systems confined to a ring have been a subject of a lot of studies during the last decade (see Ref. [83] for review). Conceptually, the distinctive feature of the ring geometry is that it is nonsimply connected. As a result, the orbital magnetism of electrons on a ring depends periodically on the magnetic flux, Φ , threading the ring. Also, as a consequence of nonsimply connectedness, the many-electron ground state on a ring becomes chiral even in a weak magnetic field, when $\Phi \ll \Phi_0$, where $\Phi_0 = hc/e$ is the flux quantum. Nontrivial magnetic and transport properties of electrons in the ring geometry become observable when the ring is small enough, so that the electron coherence length exceeds the perimeter. This condition is met at low enough temperatures. On the other hand, since the sensitivity to the flux originates from the ring geometry, it persists even if the electron elastic mean free path is smaller than the perimeter, so that the overall character of the electron transport is diffusive. The actual sizes of such rings, that were studied experimentally[83], were $\sim 10^3$ nm and more, so that the discreteness of the quantum states in these zero-dimensional objects could not be resolved.

Recently, a new technique for fabrication of the rings has been introduced[84, 85, 86, 87]. In contrast to lithography[83], this technique is based on the phenomenon of self-assembly. The rings are formed in two steps. The first step is the conventional epitaxial growth of the array of narrow gap (InAs) quantum dots on the surface of the wide-gap (GaAs) substrate. Epitaxial islands are formed spontaneously in course of this growth in order to minimize the elastic energy, caused by the 7% mismatch of the lattice constants of InAs and GaAs. These islands are then made into dots by covering them with another GaAs layer. The shape of the dots is lens (or pyramid)-like with ~ 20 nm in diameter and ~ 7 nm in height. The second step is conversion of the dots into volcano-shape rings[84, 85, 86, 87], which is achieved by annealing at the growth temperature. The rings have the height of ~ 2 nm and the outer diameter between 60 nm and 140 nm [88]. The center hole of ~ 20 nm diameter is responsible for nonsimply connectedness of the confining potential for electrons and holes.

To demonstrate that this topology indeed dramatically changes the response of electronic states in the rings to the magnetic flux, two complementary spectroscopic techniques, capacitance-voltage spectroscopy and far-infrared spectroscopy, were employed in Ref. [88]. First technique measures the magnetic-field dispersion of the ground state energy, whereas the second technique provides information about the magnetic-field dependence of the excitations. The measurements [88, 89] have revealed a cusps in charging energy and in positions of the minima in far-infrared transmission as a function of magnetic field at $\Phi \approx \Phi_0$. These cusps were identified with the change in the angular momentum of the ground state. This conclusion was supported by numerical calculations of Ref. [90], which reproduce the evolution of the peak positions in the far-infrared absorption with magnetic field.

Experimental findings of Ref. [88] have triggered theoretical studies of the single-electron states in quantum rings [91, 92]. In particular, the effect of external electric field[91] and impurity states in the ring geometry[92] were addressed. Most interesting, however, are the

many-body effects in the ring geometry.

First experimental study of the many-body effects in quantum rings was carried out in Ref. [93], where the optical emission from a charge-tunable ring was measured. Similar to [88] the tunability of the number of electrons on the ring was achieved due to the presence of a gate electrode separated from a self-assembled ring by a tunnel barrier. Changing the gate voltage allowed to add electrons to the ring one-by-one. Addition of each new electron manifested itself as a step in the capacitance-voltage characteristics. The prime observation of Ref. [93] is that all lines in the emission spectrum from the ring change abruptly upon addition of an extra electron. Photoluminescence in Ref. [93] was measured in the weak-excitation limit, which corresponds to the “classical” shakeup situation (a single hole plus degenerate electron gas). Rearrangement of the entire emission spectrum with addition of a single electron is a clear manifestation of the many-body character of the luminescence from a ring.

Lithographically fabricated[83] and self-assembled rings differ by more than an order of magnitude in diameter. Characteristic level spacing in self-assembled rings is rather large, ~ 10 meV. This fact, and the finite bandgap offsets at GaAs/InAs boundaries, restricts the maximal number of photoexcited electron-hole pairs as well as the number of electrons, injected from the gate electrode into the dot, to ~ 10 . Taking into account the spin degeneracy, the description of such a limited number of carriers in terms of a Fermi sea is hardly adequate. Therefore, in Ref. [93] the language used to interpret the many-body emission spectrum was not a shakeup (as in infinite system), but rather the electron-hole recombination in the presence of “spectators”.

Photoluminescence from quantum rings in external magnetic field is an issue of conceptual interest for the following reason. Photoexcited electron and hole form an exciton, which is a neutral entity. Neutral particle does not accumulate the Aharonov-Bohm phase in magnetic field. Therefore, it might seem that, in contrast to the infrared absorption, photoluminescence from the ring should not exhibit oscillations with period $\Phi = \Phi_0$. This is, however, not the case. The reason is that the exciton is a composite object. Therefore, even bound electron and hole can tunnel in the opposite directions and “meet” each other on the “opposite” side of the ring. This process gives rise to the flux sensitivity of the exciton. Theoretical studies of magneto-optical properties of the neutral and charged quantum ring excitons were reported in Refs. [94, 95, 96, 97, 98, 99, 100, 101, 102, 103, 104]. Moreover, the mechanism[94, 96] of the flux sensitivity of the exciton in a ring geometry was extended in Refs. [106, 107] to other neutral excitations (plasmons).

In the experimental paper Ref. [105], a weak anomaly in the luminescence spectrum of a neutral exciton in a self-assembled ring was interpreted as a possible manifestation of the Aharonov-Bohm effect.

III. LUTTINGER LIQUID THEORY OF LUMINESCENCE FROM HIGHLY EXCITED NANORINGS

A. General expression for emission rate

Here we outline the general formulas for recombination of an electron-hole pair belonging to Luttinger liquid rings in conduction and valence bands. (see Fig. 3). We start with the two-component Luttinger liquid model on a ring[108] with Hamiltonian $H_1 + H_2 + H_{int}$, where H_j describe noninteracting electrons ($j = 1$) and holes ($j = 2$) with linearized dispersions

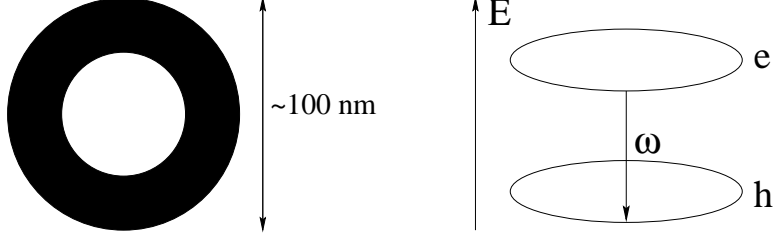


FIG. 3: Schematic representation of an electron-hole pair recombination in highly-excited Luttinger liquid ring

(the slopes are determined by the Fermi velocities v_j); H_{int} describes the interactions between carriers via screened potential $U(x)$. The electron-hole recombination rate is given by the Golden rule[16] [compare Eq. (1)]

$$W(\omega) = \frac{2\pi}{L} \sum_f |\langle f|T|i\rangle|^2 \delta(E_i - E_f - \omega) = \frac{1}{L} \int_{-\infty}^{\infty} dt e^{-i\omega t} \langle i|T^\dagger(t)T(0)|i\rangle, \quad (4)$$

where E_i and E_f are the energies of initial (ground) and final (with electron-hole pair removed) states, and

$$T = T_+ + T_-, \quad T_\pm = d \int_0^L dx \psi_{2\mp}(x) \psi_{1\pm}(x) \quad (5)$$

is the dipole transition operator. Here $\psi_{i\pm}$ are annihilation operators for left ($-$) and right ($+$) moving carriers, d is the interband dipole matrix element, and L is the ring circumference. Note that recombination occurs between left (right) electrons and right (left) holes. The recombination rate is then expressed via a four-particle Green function,

$$W(\omega) = d^2 \int_0^L dx \int_{-\infty}^{\infty} dt e^{-i\omega t} [D_+(x, t) + D_-(x, t)] = d^2 [D_+(\omega) + D_-(\omega)], \quad (6)$$

where

$$D_\pm(x, t) = \langle \psi_{2\mp}^\dagger(x, t) \psi_{1\pm}^\dagger(x, t) \psi_{1\pm}(0) \psi_{2\mp}(0) \rangle. \quad (7)$$

B. Bosonisation of electron-hole Hamiltonian

In order to evaluate $D_\pm(x, t)$ for a two-component Luttinger liquid[109, 110, 111], we use the bosonization technique on a ring[20, 80, 108]. The right/left fermion fields are presented as

$$\psi_{j\alpha}(x) = L^{-1/2} : e^{i\varphi_{j\alpha}(x)} := (2\pi\epsilon)^{-1/2} e^{i\varphi_{j\alpha}(x) + i\alpha\pi x/L}, \quad (8)$$

where ϵ is a cutoff, while right/left ($\alpha = \pm$) bosonic fields $\varphi_{j\alpha}(x)$ are related to the corresponding densities as

$$\rho_{j\alpha}(x) = \frac{\alpha}{2\pi} \frac{\partial \varphi_{j\alpha}(x)}{\partial x}. \quad (9)$$

The bosonic field has a decomposition

$$\varphi_{j\alpha}(x) = \varphi_{j\alpha}^0 + \alpha N_{j\alpha} 2\pi x/L + \bar{\varphi}_{j\alpha}(x), \quad (10)$$

where the number operator $N_{j\alpha}$ and its conjugate $\varphi_{j\alpha}^0$ satisfy the commutation relations

$$[N_{j\alpha}, \varphi_{k\beta}^0] = i\delta_{kj}\delta_{\alpha\beta}, \quad (11)$$

and the periodic field $\bar{\varphi}_{j\alpha}(x) = \bar{\varphi}_{j\alpha}(x + L)$ has a standard form,

$$\bar{\varphi}_{j\alpha}(x) = \sum_k \theta(k\alpha) \sqrt{\frac{2\pi}{L|k|}} e^{-|k|\epsilon/2} \left(e^{ikx} a_{kj} + e^{-ikx} a_{kj}^\dagger \right), \quad (12)$$

with a_{kj} and a_{kj}^\dagger satisfying boson commutation relations [$\theta(x)$ is the step function]. The boundary condition for the fermion fields, $\psi_{j\alpha}(x + L) = (-1)^{N_j} \psi_{j\alpha}(x)$, depends on the parity of the number of particles, $N_j = 2N_{j\alpha}$ ($N_{j\alpha}$ may have half-integer eigenvalues), and follows from the factorization

$$\psi_{j\alpha}(x) = L^{-1/2} : e^{\bar{\varphi}_{j\alpha}(x)} : e^{\varphi_{j\alpha}^0} e^{\alpha N_{j\alpha} 2\pi i x / L}. \quad (13)$$

The Hamiltonian $H = H_0 + H_{int}$ is quadratic in boson fields:

$$H_0 = \sum_{j\alpha} \frac{v_j}{4\pi} \int_0^L dx \left[\frac{\partial \varphi_{j\alpha}(x)}{\partial x} \right]^2, \quad (14)$$

and

$$H_{int} = \frac{1}{2} \sum_{jl} \int_0^L dx \int_0^L dy \left[\sum_\alpha \frac{\alpha}{2\pi} \frac{\partial \varphi_{j\alpha}(x)}{\partial x} \right] U_{jl}(x-y) \left[\sum_\beta \frac{\beta}{2\pi} \frac{\partial \varphi_{l\beta}(y)}{\partial y} \right], \quad (15)$$

where $U_{jl}(x)$ is the screened potential. Using Eqs. (10) and (12), the zero-modes can be separated from the bosonic part. The total Hamiltonian is then just a sum, $H = H_0 + \bar{H}$, of the zero-modes contribution,

$$H_0 = \frac{\pi}{L} \sum_{j\alpha\beta} N_{j\alpha} \left(v_j \delta_{jl} \delta_{\alpha\beta} + \frac{u_{jl}}{2} \right) N_{l\beta}, \quad (16)$$

and periodic bosonic fields contribution

$$\bar{H} = \sum_{qjl} e^{-|q|\epsilon} |q| \left[v_j \delta_{jl} a_{qj}^\dagger a_{qj} + \frac{u_{jl}}{4} (a_{qj}^\dagger + a_{-qj}) (a_{-ql}^\dagger + a_{ql}) \right], \quad (17)$$

where $u_{jl} = \pi^{-1} \int dx U_{jl}(x)$.

In order to calculate the correlation functions, the Hamiltonian \bar{H} has to be brought to the canonical form. This is done in two steps. First, we perform a two-component Bogolubov transformation in order to eliminate the cross-terms with opposite momenta,

$$a_{qj} = \sum_l (X_{jl} b_{ql} + Y_{jl} b_{-ql}^\dagger), \quad \sum_l (X_{jl} X_{ln}^\dagger - Y_{jl} Y_{ln}^\dagger) = \delta_{jn}. \quad (18)$$

We then obtain

$$\bar{H} = \sum_{qjl} e^{-|q|\epsilon} |q| b_{qj}^\dagger (X^\dagger - Y^\dagger)_{jl} v_l (X - Y)_{ln} b_{qn}, \quad (19)$$

where the matrices X and Y must satisfy

$$\sum_{lm} (X^\dagger + Y^\dagger)_{jl} (u_{lm} + v_l \delta_{lm}) (X + Y)_{mn} = \sum_l (X^\dagger - Y^\dagger)_{jl} v_l (X - Y)_{ln}. \quad (20)$$

Second, we diagonalize the Hamiltonian (19) by first presenting the matrices X and Y as

$$X = \cosh \lambda O, \quad Y = \sinh \lambda O, \quad (21)$$

where $\lambda_{jl} = \lambda_j \delta_{jl}$ is the diagonal matrix of Bogolubov angles λ_j and O is an orthogonal matrix, and then by introducing new boson operators

$$c_{qj} = \sum_l O_{jl} b_{ql}. \quad (22)$$

The Hamiltonian \bar{H} then takes the form

$$\bar{H} = \sum_{qj} e^{-|q|\epsilon} |q| \tilde{v}_j c_{qj}^\dagger c_{qj}, \quad (23)$$

with renormalized Fermi velocities

$$\tilde{v}_j = e^{-2\lambda_j} v_j. \quad (24)$$

Note that old and new boson operators are related as

$$a_{qj} = \cosh \lambda_j c_{qj} + \sinh \lambda_j c_{-qj}^\dagger. \quad (25)$$

Using the decomposition (21), Eq. (20) takes the form $\tilde{O} A O = 0$, where \tilde{O} is the transposed matrix, and the matrix A is given by

$$A_{jl} = u_{jl} e^{\lambda_j + \lambda_l} + \delta_{jl} v_j (e^{2\lambda_j} - e^{-2\lambda_j}). \quad (26)$$

The Bogolubov angles λ_j are found from the condition that all the eigenvalues of A_{jl} vanish. In a two-component case, this yields

$$e^{-2\lambda_1} = \sqrt{Q \frac{v_1 + u_{11} - v_2 Q}{v_1 Q - v_2 - u_{22}}}, \quad e^{-2\lambda_2} = Q / e^{-2\lambda_1},$$

$$Q = \sqrt{\left(1 + \frac{u_{11}}{v_1}\right) \left(1 + \frac{u_{22}}{v_2}\right) - \frac{u_{12}^2}{v_1 v_2}}. \quad (27)$$

Correspondingly, the level spacings are now $\tilde{\Delta}_j = 2\pi \tilde{v}_j / L$.

C. Calculation of the Green function

With the Hamiltonian (23), the time-dependence of new operators is standard,

$$c_{kj}(t) = e^{-i\tilde{v}_j |k| t} c_{kj}. \quad (28)$$

Using the relation (25), the periodic fields take the form

$$\bar{\varphi}_{j\alpha}(x, t) = \sum_k \sqrt{\frac{2\pi}{L|k|}} e^{-|k|\epsilon/2} \left[\theta(k\alpha) \cosh \lambda_j + \theta(-k\alpha) \sinh \lambda_j \right] \left(e^{ikx - i\tilde{v}_j|k|t} c_{kj} + e^{-ikx + i\tilde{v}_j|k|t} c_{kj}^\dagger \right). \quad (29)$$

The time-dependence of zero-modes can be easily obtained using equation of motion,

$$i\partial\varphi_{j\alpha}^0/\partial t = [\varphi_{j\alpha}^0, H_0], \quad (30)$$

with the zero-mode Hamiltonian (16). The final expression for the total time-dependent bosonic field reads

$$\varphi_{j\alpha}(x, t) = \varphi_{j\alpha}^0 + \alpha N_{j\alpha} 2\pi(x - \alpha v_j t)/L - \sum_{l\beta} u_{jl} N_{l\beta} \pi t/L + \bar{\varphi}_{j\alpha}(x, t). \quad (31)$$

We are now in position to calculate the Green functions. For this, we separate out annihilation and creation parts of the periodic field (29),

$$\bar{\varphi}_{j\alpha}(x, t) = \bar{\varphi}_{j\alpha}^-(x, t) + \bar{\varphi}_{j\alpha}^+(x, t), \quad (32)$$

which satisfy the following commutation relations

$$[\bar{\varphi}_{j\alpha}^-(x, t), \bar{\varphi}_{j\alpha}^+(x', t')] = \ln f_\alpha(z_{j\alpha} - z'_{j\alpha}) + \mu_i \ln [f_\alpha(z_{j\alpha} - z'_{j\alpha}) f_{-\alpha}(z_{j,-\alpha} - z'_{j,-\alpha})], \quad (33)$$

with

$$z_{j\alpha} = x - \alpha \tilde{v}_j t. \quad (34)$$

Then we present the fermion operator (8) in the normal-ordered form,

$$\begin{aligned} \psi_{j\alpha}(x, t) &= \psi_{j\alpha}^0(x, t) \bar{\psi}_{j\alpha}(x, t), \\ \psi_{j\alpha}^0(x, t) &= e^{iv_j(1+u_{jj}/2)\pi t/L} e^{i\varphi_{j\alpha}^0} e^{i\alpha N_{j\alpha} 2\pi z_{j\alpha}/L - i \sum_{l\beta} u_{jl} N_{l\beta} \pi t/L}, \\ \bar{\psi}_{j\alpha}(x, t) &= L^{-1/2} (2\pi\epsilon/L)^{\mu_j} e^{i\bar{\varphi}_{j\alpha}^+(x, t)} e^{i\bar{\varphi}_{j\alpha}^-(x, t)}, \end{aligned} \quad (35)$$

where we again separated out zero-mode and periodic parts. Using Eq. (35) together with commutators (11) and (33), the correlation functions can be straightforwardly calculated. For the Green function (7), we obtain

$$D_\alpha(x, t) = \left(\frac{2\pi\epsilon}{L} \right)^{2(\mu_2 + \mu_2)} \frac{e^{-it\delta_P - it\delta_u}}{L^2} [f_\alpha(z_{1\alpha})]^{1+\mu_1} [f_{-\alpha}(z_{1,-\alpha})]^{\mu_1} [f_{-\alpha}(z_{2,-\alpha})]^{1+\mu_2} [f_\alpha(z_{2\alpha})]^{\mu_2}, \quad (36)$$

where

$$\mu_i = \sinh^2 \lambda_i \quad (37)$$

is the Luttinger liquid interaction parameter, while $\delta_P = \pi(v_1 + v_2)/L$ and $\delta_u = \pi(u_{11} + u_{22} + 2u_{12})/2$ are energy shifts due the changes in the parity of electron and hole numbers and in the Coulomb energy, caused by a removal of an electron-hole pair. The coordinate dependence of $D_\alpha(x, t)$ is determined by (with $\alpha = \pm$)

$$f_\alpha(z_{j\alpha}) = \frac{1}{1 - e^{i\alpha(2\pi z_{j\alpha}/L + \alpha i\bar{c})}}, \quad (38)$$

where $\bar{\epsilon} = 2\pi\epsilon/L$ is the dimensionless cutoff. We assume that the screened interaction is the same for electrons and holes, $u_{11} = u_{22} = -u_{12} = u$, so that $\delta_u = 0$. After neglecting the parity phase δ_P (which can be absorbed into the frequency), we finally write

$$D_{\pm}(x, t) = \frac{\bar{\epsilon}^{2(\mu_2 + \mu_2)}}{L^2} [f_{\pm}(z_{1\pm})]^{1+\mu_1} [f_{\mp}(z_{1\mp})]^{\mu_1} [f_{\mp}(z_{2\mp})]^{1+\mu_2} [f_{\pm}(z_{2\pm})]^{\mu_2}. \quad (39)$$

The interaction strength is characterized by the ratio u/v_j , where

$$u = \frac{1}{\pi} \int dx U(x) \quad (40)$$

is the Fourier of screened potential; this ratio represents the average (screened) interaction in units of the (bare) level spacing near the Fermi energy. For weak interactions, $u/v_j \ll 1$, we have

$$\mu_j \simeq \left(\frac{u}{4v_j}\right)^2, \quad \tilde{\Delta}_j \simeq \Delta_j \left(1 + \frac{u}{2v_j}\right). \quad (41)$$

Note finally that the above calculation is easily generalized if the ring is penetrated by a magnetic flux ϕ . In this case, the electron and hole number operators should be shifted by flux-dependent constants, $N_{1\alpha} \rightarrow N_{1\alpha} + \alpha\phi/\phi_0$ and $N_{2\alpha} \rightarrow N_{2\alpha} - \alpha\phi/\phi_0$, where ϕ_0 is the flux quantum. This results in the replacement $\delta_P \rightarrow \delta_P(1 - 2\alpha\phi/\phi_0)$ in Eq. (36).

D. Derivation of oscillator strengths

The correlator $D_{\alpha}(x, t)$ is periodic in variables $z_{j\alpha}$. In order to carry out the integration in Eq. (6) we first perform the Fourier expansion of $[f_{\alpha}(z_{j\alpha})]^{\nu}$ as

$$[f_{\alpha}(z_{j\alpha})]^{\nu} = \sum_n b_{\nu}(n) e^{i\alpha 2\pi n z_{j\alpha}/L}, \quad b_{\nu}(n) = \frac{\sin \pi\nu}{\pi} B(n + \nu, 1 - \nu), \quad (42)$$

Substituting this Fourier expansion into Eq. (39), the Green function $D_{\alpha}(\omega)$ takes the form

$$D_{\pm}(\omega) = \bar{\epsilon}^{2(\mu_1 + \mu_2)} \sum_{\{n\}} b_{1+\mu_1}(n_1) b_{\mu_1}(n'_1) b_{1+\mu_2}(n_2) b_{\mu_2}(n'_2) \Lambda_{\pm}(\omega, \{n\}), \quad (43)$$

with

$$\begin{aligned} \Lambda_{\pm}(\omega, \{n\}) &= \frac{1}{L^2} \int dt \int_0^L dx \exp \left[-i\omega t \pm i \frac{2\pi}{L} (n_1 z_{1\pm} - n'_1 z_{1\mp} - n_2 z_{2\mp} + n'_2 z_{2\pm}) \right] \\ &= \frac{2\pi}{L} \delta_{n_1 - n'_1, n_2 - n'_2} \delta \left[\omega + \frac{2\pi \tilde{v}_1}{L} (n_1 + n'_1) + \frac{2\pi \tilde{v}_2}{L} (n_2 + n'_2) \right], \end{aligned} \quad (44)$$

where we absorbed the parity shift δ_P into ω . The Kronecker delta and the delta-function reflect the conservation of momentum and energy, respectively. Thus, we obtain

$$D_{\alpha}(\omega) = \frac{2\pi}{L} \sum_{mn} C_{mn} \delta(\omega + \tilde{\Delta}_1 m + \tilde{\Delta}_2 n), \quad (45)$$

with

$$C_{mn} = \bar{\epsilon}^{2(\mu_1 + \mu_2)} \sum_l b_{1+\mu_1}[(m+n)/2 - l] b_{1+\mu_2}(n-l) b_{\mu_1}[(m-n)/2 + l] b_{\mu_2}(l). \quad (46)$$

From Eq. (45), the emission spectrum (3) follows. Finally, using integral representation for the Beta-function in Eq. (42) we arrive at

$$C_{mn} = \int_{-\pi}^{\pi} \frac{d\phi_1 d\phi_2 d\phi_3}{(2\pi)^3} \frac{\bar{\epsilon}^{2(\mu_1 + \mu_2)} e^{-\frac{i}{2}(\phi_1 + \phi_2)(m+n) + \frac{i}{2}\phi_3(m-n)}}{(1 - e^{i\phi_1})^{1+\mu_1} (1 - e^{i\phi_2})^{1+\mu_2} (1 - e^{i(\phi_2 - \phi_3)})^{\mu_1} (1 - e^{i(\phi_1 + \phi_3)})^{\mu_2}}. \quad (47)$$

Note, that the sum in Eq. (3) is constrained by the selection rule that m and n are of the same parity, i.e., the combinations

$$N = (m+n)/2, \quad M = (m-n)/2, \quad (48)$$

which enter into the rhs of Eq. (47), are integers, as can be seen from Eq. (44). This is a result of the linear dispersion of electrons and holes near the Fermi levels.

It is easy to see that Eq. (47) correctly reproduces the non-interacting limit. Indeed, upon setting $\mu_i = 0$, the integral over ϕ_3 yields $C_{mn} = \delta_{mn}$. Another important limiting case $m, n \gg 1$ corresponds to the transitions well away from the Fermi edge. In this case, the main contribution to the integral (47) comes from the domain $\phi_1 + \phi_2 \sim (m+n)^{-1} \ll 1$. Within this domain, one can neglect the difference between ϕ_1 and $-\phi_2$ in the last two factors in the denominator. Then the integrals over ϕ_1, ϕ_2 factorize, yielding

$$C_{mn} = \frac{\Gamma(N+1+\mu_1)\Gamma(N+1+\mu_2)}{\Gamma(1+\mu_1)\Gamma(1+\mu_2)[\Gamma(N+1)]^2} K(M), \quad (49)$$

with

$$K(M) = \int_{-\pi}^{\pi} \frac{d\phi}{2\pi} \frac{\bar{\epsilon}^{2(\mu_1 + \mu_2)} e^{iM\phi}}{(1 - e^{-i\phi})^{\mu_1} (1 - e^{i\phi})^{\mu_2}} = \frac{\epsilon^{2(\mu_1 + \mu_2)} (-1)^M \Gamma(1 - \mu_1 - \mu_2)}{\Gamma(1 - M - \mu_1) \Gamma(1 + M - \mu_2)}, \quad (50)$$

where $\Gamma(x)$ is the Gamma-function. It can be seen from Eq. (50) that, for a given N , the oscillator strengths, C_{mn} , fall off as $C_{mn} \propto |M|^{\mu_1 + \mu_2 - 1}$ with increasing $|M| = \frac{1}{2}|m-n|$. This slow power-law decay reveals strong correlations within electron-hole system on a ring. Finally, using the large x asymptotics of $\Gamma(x)$, we obtain the expression for the oscillator strengths valid for $|m-n| \gg 1$,

$$C_{mn} = \frac{\bar{\epsilon}^{2\mu} \Gamma(1 - \mu)}{\Gamma(1 + \mu_1) \Gamma(1 + \mu_2)} \frac{\sin \pi \tilde{\mu}}{\pi} \left(\frac{m+n}{2}\right)^\mu \left|\frac{m-n}{2}\right|^{\mu-1}, \quad (51)$$

where

$$\mu = \mu_1 + \mu_2, \quad \tilde{\mu} = \frac{1}{2}\mu + \frac{1}{2}(\mu_1 - \mu_2) \text{sgn}(m-n). \quad (52)$$

IV. FINE STRUCTURE OF THE EMISSION SPECTRUM

The general expression (47) determines the heights of the emission peaks, while the *order* of the peaks with different $\{m, n\}$ is governed by the δ -functions in Eq. (3), which ensure the energy conservation. Therefore, this order depends crucially on the relation between $\tilde{\Delta}_1$ and $\tilde{\Delta}_2$. Moreover, a *commensurability* between $\tilde{\Delta}_1$ and $\tilde{\Delta}_2$ leads to accidental degeneracies in the positions of the emission lines. However, in order to establish the general properties of the spectrum, it is instructive to consider first several cases of commensurate $\tilde{\Delta}_1$ and $\tilde{\Delta}_2$.

A. Symmetric case

We start with the symmetric case $\tilde{\Delta}_i = \tilde{\Delta}/2$ (and, hence, $\mu_i = \mu/2$). The peak positions, as determined by Eq. (3), coincide with those for single-particle transitions, $|\omega| = N\tilde{\Delta}$. The corresponding oscillator strengths can be straightforwardly evaluated from Eq. (47) as

$$c_N = \sum_M C_{N+M, N-M} = \left[\int_{-\pi}^{\pi} \frac{d\phi}{2\pi} \frac{\bar{\epsilon}^\mu e^{-iN\phi}}{(1 - e^{i\phi})^{1+2\mu}} \right]^2. \quad (53)$$

For $N \gg 1$, the denominator of the integrand can be expanded, yielding

$$c_N \simeq (\bar{\epsilon}N)^{2\mu} = \left| \frac{\bar{\epsilon}\omega}{\tilde{\Delta}} \right|^{2\mu}. \quad (54)$$

Note that single-particle oscillator strengths correspond to $c_N = 1$. We thus conclude that interactions affect strongly the peak heights for $|\omega/\tilde{\Delta}|^{2\mu} \gg 1$, i.e., in the high frequency domain. In fact, even for an arbitrary relation between $\tilde{\Delta}_1$ and $\tilde{\Delta}_2$, the crossover between “single-particle” and “many-body” domains of the spectrum is governed by the dimensionless parameter

$$\xi = \mu \ln \frac{|\omega|}{\tilde{\Delta}_1 + \tilde{\Delta}_2}. \quad (55)$$

B. Commensurate case

Now consider the case when the level spacings in the conduction and valence band are commensurate:

$$\frac{\tilde{\Delta}_1}{\tilde{\Delta}_2} = \frac{p}{q}, \quad (56)$$

where p and q are integers. Introducing a notation

$$\tilde{\Delta} = \tilde{\Delta}_1 + \tilde{\Delta}_2, \quad (57)$$

the Green function (45) takes the form

$$D_\alpha(\omega) = \frac{2\pi}{L} \sum_{mn} C_{mn} \delta\left(\omega + \tilde{\Delta} \frac{mp + nq}{p + q}\right) = \frac{2\pi}{L} \sum_k C_k \delta(\omega + \tilde{\Delta}k/Q), \quad (58)$$

where $Q = p + q$, $P = p - q$, and

$$\begin{aligned} C_k &= \sum_{mn} \delta_{k, mp+nq} C_{mn} = \sum_{MN} \delta_{k, MP+NQ} C_{N+M, N-M} \\ &= \sum_{MN} \delta_{k-MP, NQ} C_{\frac{k}{Q}+M(1-\frac{P}{Q}), \frac{k}{Q}-M(1+\frac{P}{Q})}. \end{aligned} \quad (59)$$

Using the relation

$$\sum_N \delta_{k, NQ} = \frac{1}{Q} \sum_{l=0}^{Q-1} e^{-i2\pi lk/Q}, \quad (60)$$

the oscillator strengths can be presented as

$$C_k = \frac{1}{Q} \sum_{l=0}^{Q-1} e^{-i2\pi lk/Q} f_l(k), \quad (61)$$

with

$$f_l(k) = \sum_M e^{i2\pi lMP/Q} C_{\frac{k}{Q}+M(1-\frac{P}{Q}), \frac{k}{Q}-M(1+\frac{P}{Q})}. \quad (62)$$

Using integral representation (47), the sum over M can be explicitly performed. For $k/Q = |\omega|/\tilde{\Delta} \gg 1$, the resulting expression for coefficients f_l takes the form

$$f_l(k) = \int_{-\infty}^{\infty} \frac{d\phi_1 d\phi_2}{(2\pi)^2} \frac{\bar{\epsilon}^{2(\mu_1+\mu_2)} e^{-i(\phi_1+\phi_2)k/Q}}{(-i\phi_1)^{1+\mu_1} (-i\phi_2)^{1+\mu_2} (1-s_l - i s_l [\phi_2 + (\phi_1 + \phi_2)P/Q])^{\mu_1}} \times \frac{1}{(1-s_l^* - i s_l^* [\phi_1 - (\phi_1 + \phi_2)P/Q])^{\mu_2}}, \quad (63)$$

where $s_l = e^{i2\pi lP/Q}$. The l -dependence of $f_l(k)$ is determined by the relative magnitude of Q/k and $|1-s_l|$:

$$f_l(k) \simeq \left| \frac{\bar{\epsilon}k}{Q} \right|^{2(\mu_1+\mu_2)} \quad (64)$$

for $k/Q \ll |1-s_l|^{-1}$, and

$$f_l(k) \simeq \left(\frac{\bar{\epsilon}^2 k/Q}{1-s_l} \right)^{\mu_1} \left(\frac{\bar{\epsilon}^2 k/Q}{1-s_l^*} \right)^{\mu_2} \quad (65)$$

for $k/Q \gg |1-s_l|^{-1}$, with the two estimates matching at $k/Q \sim |1-s_l|^{-1}$.

Summarising, each "parent" single-particle peak, corresponding to $k = nQ$ in Eq. (58), acquires $Q-1$ shakeup satellites separated in energy by $\tilde{\Delta}/Q$. Such equidistant distribution of satellite positions is due to periodicity in the excitation spectrum caused by commensurate level spacings in conduction and valence band. The oscillator strengths depends strongly on frequency, $\omega/\tilde{\Delta} = k/Q$, as indicated by Eqs. (61,64,65). The emergence of satellite peaks with increasing $\omega/\tilde{\Delta}$ is demonstrated below for the simplest case when each single-particle peak acquires just one satellite.

C. Case $\tilde{\Delta}_1 = 3\tilde{\Delta}_2$

Consider now the case $\tilde{\Delta}_1 = 3\tilde{\Delta}_2$ (and thus $\mu_2 \simeq 9\mu_1$) which corresponds to the doubling of luminescence peaks number as compared to noninteracting case. Indeed, as follows from Eq. (3), here the peak spectral positions are given by

$$\frac{|\omega|}{\tilde{\Delta}} = \frac{n}{2}. \quad (66)$$

For $P = 2$ and $Q = 4$, so that $s_l = (-1)^l$, the coefficients f_l take two different values depending on the parity of l [see Eqs. (64,65)],

$$f_{\text{even}}(k) \simeq \left| \frac{\bar{\epsilon}k}{4} \right|^{2\mu} = \left| \frac{\bar{\epsilon}\omega}{\tilde{\Delta}} \right|^{2\mu}, \quad (67)$$

$$f_{\text{odd}}(k) \simeq \left| \frac{\bar{\epsilon}^2 k}{8} \right|^\mu = \left| \frac{\bar{\epsilon}^2 \omega}{2\tilde{\Delta}} \right|^\mu, \quad (68)$$

yielding [see Eq. (61)],

$$C_k = \left| \frac{\bar{\epsilon}\omega}{\tilde{\Delta}} \right|^{2\mu} \frac{1 + (-1)^k}{2} \frac{1 + e^{i\pi k/2} \left| \frac{\tilde{\Delta}}{2\omega} \right|^\mu}{2}, \quad (69)$$

with $\mu = \mu_1 + \mu_2$. Obviously, $C_k = 0$ for k odd. For k even, we have

$$C_{4l} \simeq \left| \frac{\bar{\epsilon}\omega}{\tilde{\Delta}} \right|^{2\mu} \frac{1 + \left| \frac{\tilde{\Delta}}{2\omega} \right|^\mu}{2}, \quad (70)$$

$$C_{4l+2} \simeq \left| \frac{\bar{\epsilon}\omega}{\tilde{\Delta}} \right|^{2\mu} \frac{1 - \left| \frac{\tilde{\Delta}}{2\omega} \right|^\mu}{2}, \quad (71)$$

and we finally obtain

$$D_\pm(\omega) = \frac{2\pi}{L} \left| \frac{\bar{\epsilon}\omega}{\tilde{\Delta}} \right|^{2\mu} \sum_l \left[\frac{1 + \left| \frac{\tilde{\Delta}}{2\omega} \right|^\mu}{2} \delta(\omega + \tilde{\Delta}l) + \frac{1 - \left| \frac{\tilde{\Delta}}{2\omega} \right|^\mu}{2} \delta\left[\omega + \tilde{\Delta}\left(l + \frac{1}{2}\right)\right] \right], \quad (72)$$

with $\mu = \mu_1 + \mu_2 \simeq 10\mu_1$ and $\tilde{\Delta} = \tilde{\Delta}_1 + \tilde{\Delta}_2 = 4\tilde{\Delta}_1$.

The above result illustrates how the structure of the spectrum evolves as the frequency departs from the Fermi edge. For $\xi = \mu \ln \left| \frac{\omega}{\tilde{\Delta}} \right| \ll 1$, each single-particle peak, $|\omega| = l\tilde{\Delta}$ acquires a weak shakeup satellite at $|\omega| = (l + \frac{1}{2})\tilde{\Delta}$. In the opposite limit, $\xi \gg 1$, the oscillator strength of an “integer” peak is equally redistributed between the doublet components. The crossover frequency, separating the “single-particle” and the developed many-body domains of the spectrum is determined by the condition $\xi \sim 1$, or, $\omega \sim \tilde{\Delta}e^{1/\mu}$. The spectrum (72) is schematically depicted in Fig. 4.

D. General structure of the smission spectrum

Let us turn to the structure of the spectrum in the general case of incommensurate $\tilde{\Delta}_1$ and $\tilde{\Delta}_2$. We start from the observation that the peak positions can be classified by “generations”. Namely, once a peak $\{m, 0\}$ (or $\{0, n\}$) emerges at $\omega = \omega_m = -m\tilde{\Delta}_1$ (or $\omega = \omega_n = -n\tilde{\Delta}_2$), it is followed by next generations of peaks $\omega_m^{(k)} = \omega_m - k(\tilde{\Delta}_1 + \tilde{\Delta}_2)$ or $\omega_n^{(k)} = \omega_n - k(\tilde{\Delta}_1 + \tilde{\Delta}_2)$ repeating with a period $\tilde{\Delta} = \tilde{\Delta}_1 + \tilde{\Delta}_2$. Thus, for a crude description of the spectrum away from the Fermi edge it is convenient to divide the frequency region $\omega < 0$ into the intervals of width $\tilde{\Delta}$.

The number of peaks within the spectral interval $\{-|\omega|, -|\omega| - \tilde{\Delta}\}$ is the number of integers satisfying the conditions

$$|\omega| < m\tilde{\Delta}_1 + n\tilde{\Delta}_2 < |\omega| + \tilde{\Delta}. \quad (73)$$

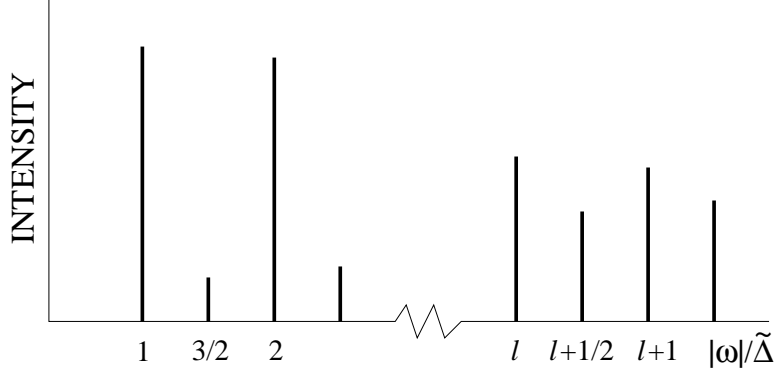


FIG. 4: Emission spectrum for $\tilde{\Delta}_1 = 3\tilde{\Delta}_2$. In low-frequency domain, the single-particle peaks acquire weak many-body shakeup satellites. In high-frequency domain, the heights of the parent ($|\omega|/\tilde{\Delta} = l$) and satellite ($|\omega|/\tilde{\Delta} = l + 1/2$) peaks are close to each other.

This number is equal to

$$\mathcal{N}_\omega = \frac{|\omega|\tilde{\Delta}}{2\tilde{\Delta}_1\tilde{\Delta}_2}, \quad (74)$$

where we assumed $|\omega| \gg \tilde{\Delta}$ and took into account the parity restriction. From Eq. (74) we find the peak density

$$g_\omega = \frac{\mathcal{N}_\omega}{\tilde{\Delta}} = \frac{|\omega|}{2\tilde{\Delta}_1\tilde{\Delta}_2}. \quad (75)$$

It also follows from Eq. (74) that

$$\delta\mathcal{N} = \mathcal{N}_{\omega-\tilde{\Delta}} - \mathcal{N}_\omega = \frac{\tilde{\Delta}^2}{2\tilde{\Delta}_1\tilde{\Delta}_2} \quad (76)$$

generations start within each interval independently of frequency. Since the heights of consecutive peaks within the interval $\tilde{\Delta}$ vary non-monotonically, it is natural to characterize these heights by the distribution function

$$F(\mathcal{C}) = \frac{1}{2g_\omega} \int_0^\infty dm dn \delta(\omega + m\tilde{\Delta}_1 + n\tilde{\Delta}_2) \delta(C_{mn} - \mathcal{C}), \quad (77)$$

where C_{mn} is given by Eq. (51). Here we made use of the fact that $\mathcal{N}_\omega \gg 1$ by treating m and n as continuous variables. The prefactor in Eq. (77) ensures the normalization ($\int_0^\infty d\mathcal{C} F(\mathcal{C}) = 1$). It is easy to see that $F(\mathcal{C})$ is nonzero in the interval $(\mathcal{C}_{min}, \mathcal{C}_{max})$, where (hereafter we omit the cutoff)

$$\mathcal{C}_{min} = \min\left\{2\mu_{1,2} \left|\frac{\tilde{\Delta}_{1,2}}{\omega}\right|^{1-2\mu}\right\}, \quad \mathcal{C}_{max} = 2\left|\frac{\omega}{\tilde{\Delta}}\right|^\mu \max\{\mu_{1,2}\}. \quad (78)$$

Within this wide interval, the distribution function falls off as

$$F(\mathcal{C}) \sim \left(\frac{\mathcal{C}_0}{\mathcal{C}}\right)^{2+\mu}, \quad \mathcal{C}_0 = \mu \left|\frac{\omega}{4} \left(\frac{1}{\tilde{\Delta}_1} + \frac{1}{\tilde{\Delta}_2}\right)\right|^{2\mu-1} \quad (79)$$

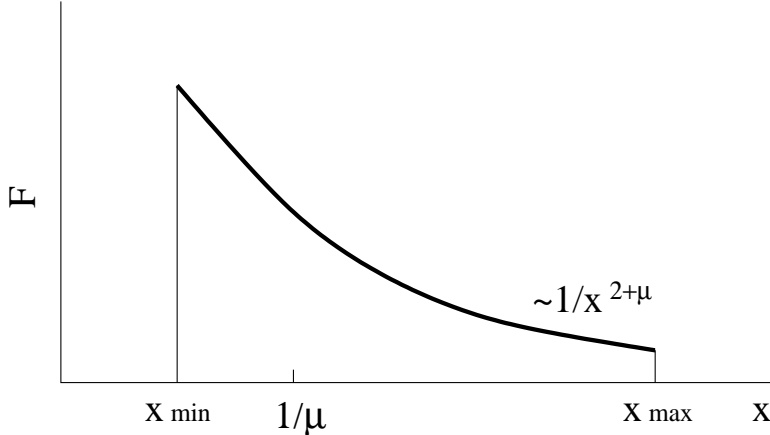


FIG. 5: The distribution function (77) of the peak heights within the interval $\tilde{\Delta}$ is plotted schematically versus $x = C/C_r$. The minimal value of x is $x_{min} \sim 1$, while $x_{max} \sim |\omega/\tilde{\Delta}|^{1-\mu} \gg 1$. The point $x = \mu^{-1}$ corresponds to the average oscillator strength.

where C_0 is the *typical* value of the oscillator strength. On the other hand, the *average* oscillator strength, which can be easily calculated from Eq. (77), is equal to $\bar{C} = \mu^{-1}C_0 \gg C_0$. The distribution function $F(C)$ is schematically depicted in Fig. 5. The fact that \bar{C} *decreases* with $|\omega|$ can be understood in the following way. As it is seen from Eq. (54), in the symmetric case, with only a single peak per interval $\tilde{\Delta}$, the peak heights increase with $|\omega|$ as $|\frac{\omega}{\tilde{\Delta}}|^{2\mu}$. In the general case, this spectral intensity gets redistributed between \mathcal{N}_ω different peaks. Thus,

$$\bar{C} \sim \mathcal{N}_\omega^{-1} \left| \frac{\omega}{\tilde{\Delta}} \right|^{2\mu} \propto |\omega|^{2\mu-1}. \quad (80)$$

V. CONCLUDING REMARKS

The underlying origin of the multitude of many-body lines in the emission spectrum from quantum-confined systems is that a recombination is accompanied by shakeup processes whose number increases as the frequency deviates from the Fermi edge. The theoretical value of the dimensionless interaction parameter μ is determined by the ratio of screened interaction U to the level spacings $\tilde{\Delta}_1$ and $\tilde{\Delta}_2$ at the corresponding Fermi levels. Both quantities depend on the number of excited carriers, N , which in turn is determined by the excitation intensity. This, and the sensitivity of the screening to the details of experimental setup, lead to a common ambiguity in the theoretical determination of μ . For example, in quantum wires, the value of μ measured in resonant tunneling experiments[112, 113], was significantly larger than theoretical estimates. Concerning the estimates for $\tilde{\Delta}_1$ and $\tilde{\Delta}_2$, in the experimental paper Ref. [93] on luminescence from ring-shape dots the total energy separation $\tilde{\Delta}$ between the lowest levels was approximately 5 meV. This value comes almost exclusively from the conduction band, due to the large ratio of the electron and hole effective masses. Both $\tilde{\Delta}_1$ and $\tilde{\Delta}_2$ increase linearly with increasing N . This implies that the shakeup processes within the hole system are experimentally much more relevant than those for electrons.

T.V.S. was supported by the Army High Performance Computing Research Center under the auspices of the Department of the Army, Army Research Laboratory under Cooperative Agreement No DAAD19-01-2-0014, and by the National Science Foundation under Grant Nos DMR-0304036 and DMR-0305557. M.E.R. was supported by the National Science Foundation under Grant No. DMR-0202790 and by Petroleum Research Fund under Grant No. 37890-AC6.

-
- [1] K. Brunner, U. Bockelmann, G. Abstreiter, M. Walter, G. Bohm, G. Trankle, and G. Weimann Phys. Rev. Lett. **69**, 3216 (1992).
 - [2] J.-Y. Marzin, J.-M. Jérard, A. Israël, D. Barrier, and G. Bastard, Phys. Rev. Lett. **73**, 716 (1994).
 - [3] A. Zrenner, J. Chem. Phys. **112**, 7790 (2000).
 - [4] D. Gammon, Nature **405**, 899 (2000).
 - [5] P. W. Anderson, Phys. Rev. Lett. **18**, 1049 (1967).
 - [6] G. D. Mahan, Phys. Rev. **153**, 882 (1967).
 - [7] P. Nozieres and C. T. de Dominicis, Phys. Rev. **178**, 1097 (1969).
 - [8] D. C. Langreth, Phys. Rev. B **1**, 471 (1970).
 - [9] R. Sooryakumar, A. Pinczuk, A. C. Gossard, D. S. Chemla, and L. J. Sham, Phys. Rev. Lett. **58**, 1150 (1987).
 - [10] A. E. Ruckenstein, S. Schmitt-Rink and R. C. Miller, Phys. Rev. Lett. **56**, 504 (1986).
 - [11] A. E. Ruckenstein and S. Schmitt-Rink, Phys. Rev. B **35**, 7551 (1987).
 - [12] M. S. Skolnick, J. M. Rorison, K. J. Nash, D. J. Mowbray, P. R. Tapster, S. J. Bass, and A. D. Pitt, Phys. Rev. Lett. **58**, 2130 (1987).
 - [13] G. Livescu, D. A. B. Miller, D. S. Chemla, M. Ramaswamy, T. Y. Chang, N. Sauer, A. C. Gossard and J. H. English, IEEE J. Quantum Electron. **24**, 1677 (1988).
 - [14] S. Schmitt-Rink, D. S. Chemla, and D. A. B. Miller, Adv. Phys. **38**, 89 (1989)
 - [15] H. Kalt, K. Leo, R. Cingolani, and K. Ploog Phys. Rev. B **40**, 12017 (1989).
 - [16] G. D. Mahan, *Many-Particle Physics* (Plenum, New York, 1990).
 - [17] K. Ohtaka and Y. Tanabe, Rev. Mod. Phys. **62**, 929, (1990).
 - [18] P. Livins and S. E. Schnatterly, Phys. Rev. B **37**, 6742 (1988).
 - [19] P. Hawrylak, Phys. Rev. B **42**, 8986 (1990).
 - [20] F. D. M. Haldane, J. Phys. C **14**, 2585 (1981).
 - [21] A. Gogolin, Phys. Rev. Lett. **71**, 2995 (1993).
 - [22] N. V. Prokof'ev, Phys. Rev. B **49**, 2148 (1994).
 - [23] C. L. Kane, K. A. Matveev, and L. I. Glazman, Phys. Rev. B **49**, 2253 (1994).
 - [24] M. Potemski, R. Stepniewski, J. C. Maan, G. Martinez, P. Wyder, and B. Etienne, Phys. Rev. Lett. **66**, 2239 (1991).
 - [25] L. V. Butov, V. I. Grinev, V. D. Kulakovskii, and T. G. Andersson Phys. Rev. B **46**, 13627 (1992).
 - [26] K. J. Nash, M. S. Skolnick, M. K. Saker, and S. J. Bass, Phys. Rev. Lett. **70**, 3115 (1993).
 - [27] M. S. Skolnick, D. J. Mowbray, D. M. Whittaker, and R. S. Smith, Phys. Rev. B **47**, 6823 (1993).

- [28] M. S. Skolnick, K. J. Nash, M. K. Saker, and S. J. Bass Phys. Rev. B **50**, 11771 (1994).
- [29] G. Finkelstein, H. Shtrikman, and I. Bar-Joseph Phys. Rev. B **56**, 10326 (1997).
- [30] J. Rubio, H. P. van der Meulen, J. M. Calleja, V. Härle, R. Bergmann, and F. Scholz, Phys. Rev. B **55**, 16390 (1997).
- [31] M. J. Manfra, B. B. Goldberg, L. Pfeiffer, and K. West, Phys. Rev. B **57**, 9467 (1998).
- [32] K. Asano and T. Ando, Phys. Rev. B **65**, 115330 (2002).
- [33] T. Uenoyama and L. J. Sham, Phys. Rev. B **39**, 11044 (1989).
- [34] S. Katayama, T. Ando, Solid State Commun. **70**, 97 (1989).
- [35] P. Hawrylak, Phys. Rev. B **44**, 11236 (1991).
- [36] In strong magnetic field, valence band mixing can give rise to interband transitions with different Landau levels, see S.-R. E. Yang and L. J. Sham, Phys. Rev. Lett. **58**, 2598 (1987).
- [37] I. V. Lerner and Yu. E. Lozovik, Zh. Exp. Teor. Fiz. **80**, 1488 (1981) [Sov. Phys.-JETP **53**, 763 (1981)].
- [38] S. Glasberg, H. Shtrikman, and I. Bar-Joseph, Phys. Rev. B **63**, 201308 (2001).
- [39] M. Kubisa, L. Bryja, K. Ryczko, J. Misiewicz, C. Bardot, M. Potemski, G. Ortner, M. Bayer, A. Forchel, and C. B. Srensen, Phys. Rev. B **67**, 035305 (2003).
- [40] L. Gravier, M. Potemski, P. Hawrylak, and B. Etienne, Phys. Rev. Lett. **80**, 3344 (1998).
- [41] L. Osborne, A. J. Shield M. Y. Simmons, N. R. Cooper, D. A. Ritchie, and M. Pepper, Phys. Rev. B **58**, 4427 (1998).
- [42] S. Takeyama, G. Karczewski, T. Wojtowicz, J. Kossut, H. Kunimatsu, K. Uchida, and N. Miura, Phys. Rev. B **59**, 7327 (1999).
- [43] F. M. Munteanu, Y. Kim, C. H. Perry, D. Heiman, D. G. Rickel, M. Sundaram, and A. C. Gossard, Phys. Rev. B **62**, 4249 (2000).
- [44] N. R. Cooper and D. B. Chklovskii, Phys. Rev. B **55**, 2436 (1997).
- [45] P. Hawrylak and M. Potemski, Phys. Rev. B **56**, 12 386 (1997).
- [46] Y. Kim, F. M. Munteanu, C. H. Perry, D. G. Rickel, J. A. Simmons, L. N. Pfeiffer, and K. W. West, Phys. Rev. B **64**, 195302 (2001).
- [47] F. Plentz, D. Heiman, L. N. Pfeiffer, and K. W. West, Phys. Rev. B **57**, 1370 (1998).
- [48] A. Zangwill and P. Soven, Phys. Rev. B **24**, 4121 (1981).
- [49] F. Gel'mukhanov and H. Agren, Phys. Rep. **312**, 87 (1999).
- [50] G. B. Armen, H. Aksela, T. Aberg, S. Aksela, J. Phys. B **33**, R49 (2000).
- [51] M. Ikezawa, Y. Masumoto, T. Takagahara, and S. V. Nair, Phys. Rev. Lett. **79**, 3522 (1997).
- [52] L. Landin M. S. Miller, M.-E. Pistol, C. E. Pryor, and L. Samuelson, Science, **280**, 262 (1998).
- [53] M. Bayer, T. Gutbrod, A. Forchel, V. D. Kulakovskii, A. Gorbunov, M. Michel, R. Steffen, and K. H. Wang, Phys. Rev. B **58**, 4740 (1998).
- [54] V. D. Kulakovskii, G. Bacher, R. Weigand, T. Kummell, A. Forchel, E. Borovitskaya, K. Leonardi, and D. Hommel, Phys. Rev. Lett. **82**, 1780 (1999).
- [55] E. Dekel, D. Gershoni, E. Ehrenfreund, D. Spector, J. M. Garcia, and P. M. Petroff, Phys. Rev. Lett. **80**, 4991 (1998).
- [56] E. Dekel, D. Gershoni, E. Ehrenfreund, J. M. Garcia, and P. M. Petroff, Phys. Rev. B **61**, 11 009 (2000).
- [57] E. Dekel, D. V. Regelman, D. Gershoni, E. Ehrenfreund, W. V. Schoenfeld, and P. M. Petroff, Phys. Rev. B **62**, 11038 (2000).
- [58] F. Findeis, A. Zrenner, G. Bohm, and G. Abstreiter, Solid State Commun. **114**, 227 (2000).
- [59] M. Bayer, O. Stern, P. Hawrylak, S. Fafard, and A. Forchel, Nature **405**, 923 (2000).

- [60] E. Dekel, D. V. Regelman, D. Gershoni, E. Ehrenfreund, W. V. Schoenfeld, and P. M. Petroff, *Solid State Commun.* **117**, 395 (2001).
- [61] D. V. Regelman, U. Mizrahi, D. Gershoni, E. Ehrenfreund, W. V. Schoenfeld, and P. M. Petroff, *Phys. Rev. Lett.* **87**, 257401 (2001).
- [62] D. V. Regelman, E. Dekel, D. Gershoni, E. Ehrenfreund, A. J. Williamson, J. Shumway, A. Zunger, W. V. Schoenfeld, and P. M. Petroff, *Phys. Rev. B* **64**, 165301 (2001).
- [63] K. Hinzer, P. Hawrylak, M. Korkusinski, S. Fafard, M. Bayer, O. Stern, A. Gorbunov, and A. Forchel, *Phys. Rev. B* **63**, 075314 (2001).
- [64] M. Bayer, G. Ortner, O. Stern, A. Kuther, A. A. Gorbunov, A. Forchel, P. Hawrylak, S. Fafard, K. Hinzer, T. L. Reinecke, S. N. Walck, J. P. Reithmaier, F. Klopff, and F. Schfer, *Phys. Rev. B* **65**, 195315 (2002).
- [65] P. Hawrylak, *Phys. Rev. B* **60**, 5597 (1999).
- [66] M. Combescot and P. Nozieres, *J. Phys (Paris)* **32**, 913 (1971).
- [67] P. Hawrylak, *Phys. Rev. B* **44**, 3821 (1991)
- [68] S. A. Brown, J. F. Young, J. A. Brum, P. Hawrylak, and Z. Wasilewski, *Phys. Rev. B* **54**, 11082 (1996); **56**, 1637 (1997).
- [69] V. Huard, R. T. Cox, K. Saminadayar, A. Arnoult and S. Tatarenko, *Phys. Rev. Lett.* **84**, 187 (2000).
- [70] G. Yusa, H. Shtrikman, and I. Bar-Joseph, *Phys. Rev. B* **62**, 15390 (2000).
- [71] K. Kheng, R. T. Cox, Merle Y. d' Aubignè, Franck Bassani, K. Saminadayar, and S. Tatarenko, *Phys. Rev. Lett.* **71**, 1752 (1993).
- [72] G. Finkelstein, H. Shtrikman, and I. Bar-Joseph *Phys. Rev. Lett.* **74**, 976 (1995)
- [73] A. J. Shields, M. Pepper, M. Y. Simmons, and D. A. Ritchie, *Phys. Rev. B* **52**, 7841 (1995).
- [74] G. Finkelstein, H. Shtrikman, and I. Bar-Joseph, *Phys. Rev. B* **53**, 12593 (1996).
- [75] J. R. Chapman, N. F. Johnson, and V. N. Nicopoulos *Phys. Rev. B* **57**, 1762 (1998).
- [76] Y. Toda, O. Moriwaki, M. Nishioka, and Y. Arakawa, *Phys. Rev. Lett.* **82**, 4114 (1999).
- [77] L. V. Butov, V. D. Kulakovskii, E. Lach, A. Forchel, and D. Grtzmacher, *Phys. Rev. B* **44**, 10680 (1991).
- [78] L. V. Butov, V. D. Egorov, V. D. Kulakovskii, and T. G. Andersson, *Phys. Rev. B* **46**, 15156 (1992).
- [79] S. Glasberg, H. Shtrikman, and I. Bar-Joseph, *Phys. Rev. B* **63**, 113302 (2001)
- [80] T. V. Shahbazyan, I. E. Perakis, and M. E. Raikh, *Phys. Rev. B* **64**, 115317 (2001).
- [81] M. Sassetti and B. Kramer, *Phys. Phys. Lett.* **80**, 1485 (1998).
- [82] B. Kramer and M. Sassetti, *Phys. Phys. B* **62**, 4238 (2000).
- [83] C. Chapelier, D. Mailly, and A. Benoit, *Adv. Solid State Phys.* **34**, 163 (1995).
- [84] J. M. Garcia, G. Medeiros-Ribeiro, K. Schmidt, T. Ngo, J. L. Feng, A. Lorke, J. Kotthaus, and P. M. Petroff, *Appl. Phys. Lett.* **71**, 2014 (1997).
- [85] A. Lorke and R. J. Luyken, *Physica B* **256**, 424 (1998).
- [86] A. Lorke, R. J. Luyken, M. Fricke, J. P. Kotthaus, G. Medeiros-Ribeiro, J. M. Garcia, and P. M. Petroff, *Microelectron. Eng.* **47**, 95 (1999).
- [87] H. Pettersson, R. J. Warburton, A. Lorke, K. Karrai, J. P. Kotthaus, J. M. Garcia, and P. M. Petroff, *Physica E (Amsterdam)* **6**, 510 (2000).
- [88] A. Lorke, R. J. Luyken, A. O. Govorov, J. P. Kotthaus, J. M. Garcia, and P. M. Petroff, *Phys. Rev. Lett.* **84**, 2223 (2000).
- [89] P. M. Petroff, A. Lorke, and A. Imamoglu, *Physics Today*, **54**, 46 (2001).
- [90] A. Emperador, M. Pi, M. Barranco, and A. Lorke, *Phys. Rev. B* **62**, 4573 (2000).

- [91] Z. Barticevic, G. Fuster, and M. Pacheco, Phys. Rev. B **65**, 193307 (2002).
- [92] B. S. Monozon and P. Schmelcher, Phys. Rev. B **67**, 045203 (2003).
- [93] R. J. Warburton, C. Schflein, D. Haft, F. Bickel, A. Lorke, K. Karrai, J. M. Garcia, W. Schoenfeld, and P. M. Petroff, Nature (London) **405**, 926 (2000).
- [94] A. V. Chaplik JETP Lett. **62**, 900 (1995).
- [95] A. V. Chaplik and A. O. Govorov, Physica B **256/258**, 477 (1998).
- [96] R. A. Römer and M. E. Raikh, Phys. Rev. B **62**, 7045 (2000).
- [97] R. A. Römer and M. E. Raikh, Phys. Status Solidi (b) **221** 535 (2000)
- [98] H. Hu, D.-J. Li, J.-L. Zhu and J.-J. Xiong, J. Phys.: Condens. Matter **12**, 9145 (2000).
- [99] H. Hu, G.-M. Zhang, J.-L. Zhu, and J. J. Xiong, Phys. Rev. B **63**, 045320 (2001).
- [100] R. A. Römer and M. E. Raikh, Phys. Status Solidi (b) **227**, 381 (2001).
- [101] T. Meier, P. Thomas, and S. W. Koch, Eur. Phys. J. B **22**, 249 (2001).
- [102] J. Song and S. E. Ulloa, Phys. Rev. B **63**, 125302 (2001).
- [103] H. Hu, J.-L. Zhu, D.-J. Li, and J.-J. Xiong, Phys. Rev. B **63**, 195307 (2001).
- [104] A. O. Govorov, S. E. Ulloa, K. Karrai, R. J. Warburton, Phys. Rev. B **66**, 081309(R) (2002).
- [105] D. Haft, C. Schulhauser, A. O. Govorov, R. J. Warburton, K. Karrai, J. M. Garcia, W. Schoenfeld, P. M. Petroff, Physica E **13**, 165 2002
- [106] A. I. Vedernikov, A. O. Govorov, and A. V. Chaplik, JETP **93**, 853 (2001).
- [107] A. V. Chaplik, JETP Lett. **75**, 292 (2002).
- [108] T. V. Shahbazyan and S. E. Ulloa, Phys. Rev. B **55**, 13702 (1997).
- [109] I. E. Dzyaloshinsky and A. I. Larkin, Zh. Eksp. Teor. Fiz. **65**, 411 (1974) [Sov. Phys. JETP **38**, 202 (1974)].
- [110] K. A. Matveev and L. I. Glazman, Phys. Rev. Lett. **70**, 990 (1993).
- [111] K. Penc and J. Sólyom, Phys. Rev. B **47**, 6273 (1993).
- [112] O. M. Auslaender, A. Yacoby, R. de Picciotto, K. W. Baldwin, L. N. Pfeiffer, K. W. West, Phys. Rev. Lett. **84**, 1764 (2000).
- [113] T. Kleimann, M. Sasseti, B. Kramer, and A. Yacoby, Phys. Rev. B **62**, 8144 (2000).